Journal of Alloys and Compounds 509 (2011) 9849–9857

Contents lists available at ScienceDirect

Journal of Alloys and Compounds

journal homepage: www.elsevier.com/locate/jallcom

# Synthesis, characterization, magnetic and electrical properties of the novel conductive and magnetic Polyaniline/$MgFe_2O_4$ nanocomposite having the core–shell structure

Rasha M. Khafagy

*Materials Science Laboratory, Physics Department, Girls College for Arts, Science, and Education, Ain Shams University, Cairo, Egypt*

ARTICLE INFO

*Article history:*
Received 1 January 2011
Received in revised form 2 July 2011
Accepted 5 July 2011
Available online 12 July 2011

*Keywords:*
Nanocomposite
Core–shell
In situ chemical polymerization Polyaniline
Magnesium ferrite
Magnetic and electrical properties
Thermal stability
TEM
Raman characterization

ABSTRACT

Conductive and magnetic Polyaniline/$MgFe_2O_4$ nanocomposite was successfully synthesized in the form of core–shell via in situ chemical polymerization of aniline in the presence of $MgFe_2O_4$ nano-particles. X-ray powder diffraction of ferrites indicated that the structure of the core material is having the spinel structure, and demonstrated the formation of PAni/$MgFe_2O_4$ nanocomposite. XRD and TEM photographs showed that the particle's size of the $MgFe_2O_4$ core-material were around 30–35 nm before coating with Polyaniline, and grown up to 45 nm in the core–shell nanocomposite after coating. Although PAni has a relatively smaller electrical field coefficient than the core–shell nanocomposite, the resistivity of the core–shell material decreased, and hence its conductivity increased after a certain threshold voltage of 0.98 V equivalent to threshold electric field value equals 5.5 V $cm^{-1}$. The magnetic hysteresis loops investigated with VSM indicated that coating $MgFe_2O_4$ with Polyaniline has an healing effect which covers the ferrite surface defects, thus decreasing the magnetic surface anisotropy of ferrite particles leading to a decrease of the saturated magnetization (Ms) from 21.33 emu/g to 5.905 emu/g and a decrease of the coercivity (Hc) from 88.66 Oe to 81.6 Oe for $MgFe_2O_4$ and the core–shell nanocomposite respectively due to the amount of Polyaniline added. TGA and DTA revealed improved thermal stability of the core–shell nanocomposite with respect to that of Polyaniline due to the incorporation of ferrites. Raman spectroscopy confirmed TGA, DTA and XRD studies, and revealed that pure PAni is less stable than the corresponding core–shell nanocomposite with respect to molecular changes which might occur during heating at elevated temperatures. Moreover, Raman study confirmed the interfacial interaction between the core and the shell materials, and lead to an assumption about the presence of different conjugation chain lengths and types, such as the presence of the semi-quinones aside the quinone rings in the polymer chain, which showed different response upon heating the sample.



## 1. Introduction

Conducting polymer nanocomposites especially when incorporated with inorganic magnetic oxides have attracted considerable interest because of their potential for combining properties that are difficult to attain separately with the individual components [1]. The main idea in a composite is to integrate several component materials and their properties in a single material [2]

The need for combining the magnetic properties with the conductive properties leads to processing new materials such as conductive polymers with magnetic behavior, or magnetic particles containing a conductive polymer [3]. Such new materials have attracted more and more attention due to their unique properties and their potential application as batteries, electrochemical display devices, electrical-magnetic shields and microwave absorption materials [4–9].

A feasible route to combine the magnetic properties with the conductive properties is to prepare magnetic particle/conductive polymer nanocomposites, which has led to a new coating strategy using inherently conducting polymer as a key component which surrounds ferromagnetic material [10]. Materials comprising a ferromagnetic component and a conducting polymer have recently been investigated in several studies that concentrated on the preparation of nano-colloidal iron oxides, $\gamma$-$Fe_2O_3$ [11] and $Fe_3O_4$ [12,13], and their subsequent modification with conducting polymers. Although such composites have been successfully prepared by several groups [14–16], but, the magnetic and conductive properties of the prepared materials were relatively poor due to either the synthetic methods or the used materials.

*E-mail address:* RashaKhafagy@hotmail.com

0925-8388/$ – see front matter © 2011 Elsevier B.V. All rights reserved.
doi:10.1016/j.jallcom.2011.07.008

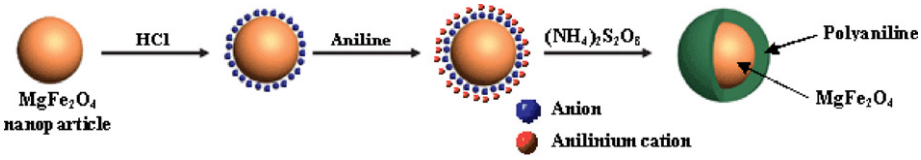


**Fig. 1.** The polymerization procedures for PAni/$MgFe_2O_4$ core shell nanocomposite.

In this paper it is aimed to synthesize a novel electrical/magnetic nanocomposite with an interesting well-designed core–shell structure and specific good magnetic and conductive properties, which are difficult to be combined together. It is chosen here to combine the intrinsically conducting polymer Polyaniline (PAni) with the magnetic material $MgFe_2O_4$ due to the specific and unique properties of each.

Intrinsically conducting polymers (ICPs), among them PAni, are a novel class of synthetic materials that have both the electrical and optical properties of semiconductors and metals, together with the mechanical properties and high processability of polymers. Also, a high level of conductivity (near metallic) can be achieved in ICPs through oxidation–reduction as well as doping with a suitable dopant [17]. That is why those polymers have become a popular basic material for advanced applications [18]. Although, a variety of ICPs which have been synthesized and investigated, Polyaniline and its derivatives has emerged as the most promising conducting polymer due to its unique electrical, optical and opto-electrical properties, its straight forward and easy polymerization, in addition to its excellent environmental stability [18].

On the other hand, spinel ferrites of the type $MFe_2O_4$ (M is a divalent metal cation) are currently key materials for advancements in electronics, magnetic storage, ferro-fluid technology, and many bio-inspired applications such as drugs carriers for magnetically guided drug delivery and as contrast agents in magnetic resonance imaging [19].

In this study, an approach was reported to synthesize a magnetic and conductive PAni/$MgFe_2O_4$ nanocomposite having the novel core–shell structure by in situ polymerization of aniline with $MgFe_2O_4$ nano-particles. The coating method of magnetic ferrite nano particles with PAni is reported here and well analyzed. The structure, particle sizes, as well as thermal, and surface properties of the resultant PAni/$MgFe_2O_4$ core–shell nanocomposite were characterized and reported. The magnetic and conductive properties of the novel PAni/$MgFe_2O_4$ nanocomposite were investigated and explained due to new possible surface, inter-facial, inter-particles, and exchange interactions between the magnetic nano-particles and the conductive polymer matrix.

We aim in this paper to synthesize a novel electrical/magnetic core–shell nanocomposite showing specific good conductive properties, and tunable magnetic properties which might lead to the fabrication of specially tailored material suitable for demanding applications. Amazingly, adding nano ferrite to PAni increased its thermal stability, enhanced its electrical conductivity, and the magnetic saturation of the core–shell nanocomposite could be tuned and tailored depending on the volume fraction of the magnetic ferrite nano-particles and the contribution of the non-magnetic PAni coating layer to the total magnetization.

## 2. Materials and Methods

### 2.1. Preparation of $MgFe_2O_4$ nano-particles

$MgFe_2O_4$ nano-particles were prepared by mixing a solution of $Mg(NO_3)_2{\cdot}6H_2O$ (10.723 g/250 mL) and $Fe(NO_3)_3{\cdot}9H_2O$ (33.91 g/250 mL) in de-ionized water with a solution containing 1:1 NaOH + $Na_2CO_3$ [20,21] ([NaOH] = 1.6 [$Mg^{2+}$ + $Fe^{3+}$], [$CO_3^{2+}$] = 2.0 [$Fe^{3+}$]) in de-ionized water (pH ≈ 9). The solutions were simultaneously added to a colloid mill [22,23] and mixed for 2 min. The resulting slurry was placed in a three neck flask and aged at 100 °C for 6 hrs in a Thermo Scientific Heraeus M104 Muffle Furnace, with heating rate 4 °C/min. The final precipitate was filtered, washed thoroughly with de-ionized water and dried at 100 °C for 24 h. The resulting sample was then calcined at 900 °C for 2 h inside the M104 Muffle Furnace at a heating rate of 4 °C/min and then grinded to obtain the fine nano-powder.

### 2.2. Synthesis of PAni/$MgFe_2O_4$ core–shell nanocomposite

A typical in situ chemical polymerization method for the PAni/$MgFe_2O_4$ was carried out by the routine synthesis [24]. 0.5 g of $MgFe_2O_4$ was added to 50 mL of freshly prepared reaction mixture (0.2 M aniline and 0.25 M ammonium peroxydisulphate in 1 M HCl) at 20 °C. The mixture was stirred during the polymerization of aniline for 12 h. The ferrite coated with PAni was separated on a filter paper, rinsed with 1 M HCl and warm de-ionized water, and then dried at 70 °C in an electrical oven M104 Muffle Furnace at a heating rate of 4 °C/min.

The polymerization procedures for PAni/$MgFe_2O_4$ core shell nanocomposite are shown in Fig. 1 as described in [24]. Since the surface charge of the metal oxide is positive in acidic conditions, so, an amount of $Cl^-$ is adsorbed on the ferrite surface to compensate the positive charges. In the same acidic conditions the aniline monomers are converted to cationic anilinium ions, this leads to the electrostatic interactions produced between the adsorbed anions and cationic anilinium ions. Then the $(NH_4)_2S_2O_8$ is used as oxidizing agent to polymerize the adsorbed ions on the ferrite particles producing the PAni/$MgFe_2O_4$ nanocomposite.

### 2.3. Sample analysis

The $MgFe_2O_4$, PAni and PAni/$MgFe_2O_4$ nanocomposite were identified by X-ray Philips analytical (X'pert Graphics & Identify) diffractometer, and the average crystallite size was computed using the associated software facility by applying Scherer's formula [25].

Morphology of the nanocomposite was observed using TEM (JEOL JEM-1230). The magnetic properties were investigated by Vibrating Sample Magnetometer model 9600, while the electrical measurements were conducted using a Keithley Instrument, Inc. 6514 electrometer and resistivity cell after compressing PAni and PAni/$MgFe_2O_4$ nanocomposite into pillets. The thermal analysis was performed using MAC-science model DTA-TG2000, and the Raman study was performed on ThermoFisher Scientific, Italy, DXR dispersive Raman Microscope with integrated components: laser, grating, Rayleigh filters, spectrograph, research-class optics and microscope with binocular and digital camera. Raman software communication is established through a single USB port that controls video, stage and CCD detector.

## 3. Results and discussion

### 3.1. X-ray diffraction

Crystallinity and orientation of conducting polymer have been of interest, because more highly ordered system could display a metal-like conducting state [26]. Fig. 2a and b illustrates the XRD patterns for $MgFe_2O_4$, PAni, and PAni/$MgFe_2O_4$ core–shell nanocomposite. For clarity, Fig. 2a represents separated XRD patterns for the three samples, while Fig. 2b represents overlaid XRD patterns, where the prominent peaks of $MgFe_2O_4$, PAni and the core–shell nanocomposite of both are reported.

#### 3.1.1. X-ray diffraction of pure $MgFe_2O_4$, and pure PAni parents

The XRD pattern of $MgFe_2O_4$ consists of well-resolved broad peaks, which confirms the polycrystalline and mono-phasic nature of the prepared nano-ferrite material. The XRD diffraction peaks correspond to planes (2 2 0), (3 1 1), (2 2 2), (4 0 0), (4 2 2), (3 3 3), (4 4 0), (6 2 0) and (5 3 3). Obtained $2\theta$ peaks provide a clear evidence for the formation of single phase spinel structure of ferrite [27]. This observation matches well with those of earlier reporters [28,29], and with the ICDD card number (73-1720) used in identifying X-ray pattern, in addition to JCPDS (73-2410) file for $MgFe_2O_4$.

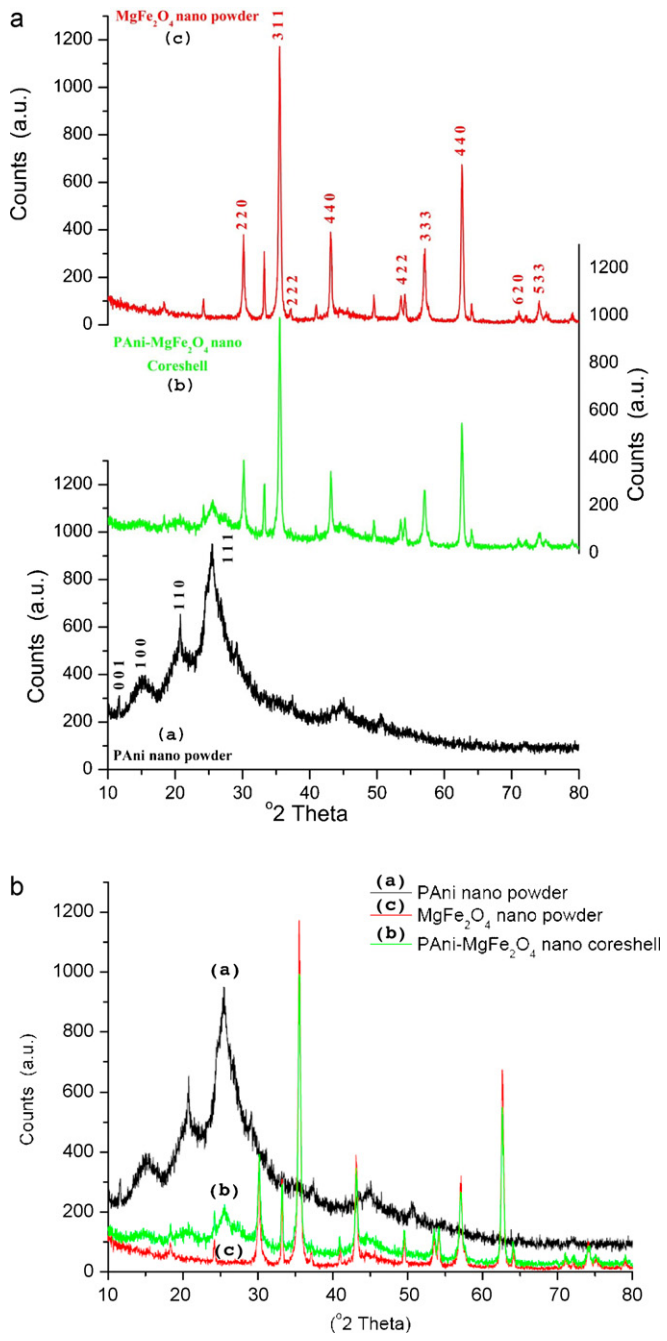


**Fig. 2. (a)** Vertically separated X-ray diffraction patterns for: (a) PAni, (b) PAni/$MgFe_2O_4$ core shell nanocomposite and (c) $MgFe_2O_4$ nano-particles. **(b)** Overlaid X-ray diffraction patterns for: (a) PAni, (b) PAni/$MgFe_2O_4$ core shell nanocomposite and (c) $MgFe_2O_4$ nano-particles.

The crystallite size (L) of $MgFe_2O_4$ nano particles calculated from XRD pattern is about 33 nm.

The PAni nano-particles exhibit several diffraction peaks at $2\theta = 11.7^\circ$ ($d = 7.57$ Å), $2\theta = 15^\circ$ ($d = 5.86$ Å), $2\theta = 20.8^\circ$ ($d = 4.27$ Å), and $2\theta = 24.5^\circ$ ($d = 3.6$ Å), attributed to the (0 0 1), (1 0 0), (1 1 0) and (1 1 1) reflections of PAni as consistent with literature [30–32]. This indicates that PAni is present in the semi-crystalline ES-I type corresponding to the diffraction plane of ES-I structure of HCl doped PAni, at which the unit cell contains a single polymer zigzag and a chloride anion in a very compact packing [25]. The main reflections observed for PAni can be then indexed in a pseudo-orthorhombic cell [25].

The two diffraction peaks at $2\theta = 20.8^\circ$ and $2\theta = 24.5^\circ$ are ascribed to periodicity parallel and periodicity perpendicular to the polymer chain, respectively [33]. The peak at $2\theta = 20.8^\circ$ also represents the characteristic distance between the ring planes of benzene rings in adjacent chains or the close contact inter-chain distance [34].

### 3.1.2. X-ray diffraction of PAni/$MgFe_2O_4$ core–shell nanocomposite

The XRD spectrum of PAni/$MgFe_2O_4$ core–shell nanocomposite shows that the diffraction peaks are just the superposition of those for Polyaniline and Magnetic ferrite nano-particles. This indicates the formation of PAni/$MgFe_2O_4$ nanocomposite. As there are no new peaks appearing in the core–shell spectrum, therefore no additional crystalline order is introduced into the nanocomposite.

Even though, it is obvious that the crystalline behavior of PAni is so much affected by adding $MgFe_2O_4$ to its core. The XRD pattern for the PAni/$MgFe_2O_4$ core–shell shows much weaker PAni diffraction peaks, and the diffraction pattern of the core–shell composite is more likely that of $MgFe_2O_4$. This means that $MgFe_2O_4$ retains its spinel structure even though it gets dispersed in aniline before polymerization. Also, the reduction of the PAni diffraction peak at $2\theta = 20.8^\circ$ in the composite, suggests that X-ray scattered from magnesium atoms in $MgFe_2O_4$ is more prominent than X-ray scattered from C, H and N-atoms in the PAni polymer.

However, some characteristic peaks of PAni are still appearing in the XRD spectrum of the core–shell, this means that when Polyaniline deposits on the surface of nano-$MgFe_2O_4$, the crystalline behavior of Polyaniline is hampered and the degree of crystallinity decreases. Therefore, lower intensity of PAni peaks is due to the presence of large amounts of $MgFe_2O_4$ nano powder in the PAni matrix. In addition to this dilution effect, it seems plausible to assume that the incorporation of $MgFe_2O_4$ within PAni prevents its chains from extending and inhibits its crystallization. This means that the polymer became almost completely amorphous after coating the $MgFe_2O_4$ nano-particles. Vise versa, the Polyaniline coating layer has an effect on the crystallinity of $MgFe_2O_4$, as the intensities of most diffraction peaks corresponding to magnetic ferrite in the core–shell nanocomposite became weaker than that of pure magnetic ferrite nano-particles. This behavior is very clear in Fig. 2b.

Hence, XRD gave an evidence about the formation of PAni/$MgFe_2O_4$ nanocomposite because no peak shift and no additional peaks were found in the XRD spectrum of the obtained material. Also, XRD study suggests that PAni undergoes interfacial interactions with $MgFe_2O_4$ crystallites and loses its own morphology by coating the magnetic ferrite nano-crystallites, which is in consistent with TGA results given below. This implies that there is no strong chemical interaction between PAni and $MgFe_2O_4$ in the prepared core–shell nanocomposite.

The average crystallite sizes of $MgFe_2O_4$ nano-particles, and the PAni/$MgFe_2O_4$ core–shell nanocomposite were estimated from the X-ray diffraction patterns using Scherrer formula [35]:

$$D = \frac{k\lambda}{\beta \cos\theta}$$

where $D$ is the average crystallite size, $\lambda$ is the X-ray wavelength, $\beta$ is the full-width at half-maximum (FWHM) and $\theta$ is the diffraction angle. The value of $k$ depends on several factors, including the Miller index of reflection plane and the shape of the crystal. If shape is unknown, $k$ is often assigned a value of $0.89 \approx 0.9$. So the crystallite size of $MgFe_2O_4$ nano-particles, and the PAni/$MgFe_2O_4$ core–shell nanocomposite was computed from XRD patterns and found to be about 33 nm, 45 nm respectively.

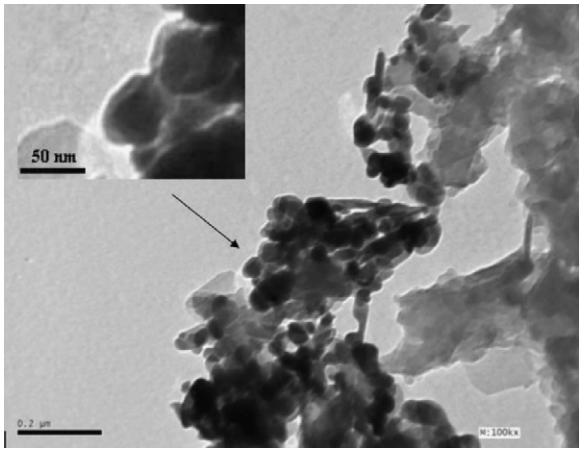


**Fig. 3.** TEM image for PAni/$MgFe_2O_4$ core–shell nanocomposite.

### 3.2. TEM

The morphology and particle size of PAni/$MgFe_2O_4$ core–shell nanocomposite were revealed by the TEM image shown in Fig. 3. TEM image shows that the ferrite nano-particles are embedded in the PAni matrix forming the interesting core–shell structure. The dark core is the ferrite nano-particles with diameter in the range of 30–35 nm, and the light colored shell is the PAni shell in the nanocomposite. The particle size of the core–shell nanocomposite are around 45 nm. The difference in colors between the core and the shell is due to the different electron penetrability. The crystallite size determination of the nano-ferrite, nano-polymer and the core–shell nano-composite was ensured mathematically by Scherer's equation, using the band height and width of the XRD patterns.

### 3.3. Thermal analysis

Thermal studies of PAni conducting polymers are particularly important when it is considered to use elevated temperatures to process PAni and its blends into technologically useful forms. In any practical application, knowledge of the stability and degradation mechanism of this class of conducting polymers is also of primary importance, such as the use of PAni's in battery applications, where the thermal stability of the material is very important. It has been reported by several researchers that a good thermal stability of PAni could be improved by combining PAni with multi-walled carbon nanotubes or nano-ZnO particles. In this piece of work, TGA analysis was carried out to study the thermal stability of the prepared PAni/$MgFe_2O_4$ core–shell nanocomposite known as intercalated system, since it is thought that the core material might act as an oxidizing agent and might affect the thermal stability of PAni. Thermograms of core–shell were carefully compared with that of the pure PAni. Two sets of samples including untreated and pre-heated pure PAni nano-particles, and core–shell nanocomposite were subjected to thermal investigations.

#### 3.3.1. Thermal behavior of untreated PAni nano-particles

Fig. 4a shows TGA and DrTGA curve of pure untreated PAni nano-particles. Pure PAni usually undergoes several stages of weight loss corresponding to the release of water and chain decomposition on being heated to elevated temperature [36].

The first continuous weight loss is observed above room temperature up to 110 °C and may be attributed to the loss of volatilized moisture, free HCl and un-reacted monomer. This first stage of weight loss has a corresponding endothermic peak in the DTA curve and its derivative curve given in Fig. 5a and b, respectively.

The second weak endothermic peaks at 130 °C and 204 °C are possibly generated by either re-crystallization and/or crosslinking reactions of PAni chains which is actually crucial to conducting polymers [36]. In addition, possible loss of HCl dopants from deeper sites in the material could take place within this second stage of weight loss. Also, the second stage of weight loss has a corresponding endothermic peak in the DTA curve and its derivative curve given in Fig. 5a and b, respectively.

At more extreme temperatures, the third weight loss ranging from 280 °C to 600 °C appeared due to polymer backbone degradation which might be accompanied by the production of gases such as acetylene, ammonia and carbon dioxide. Our data is in consistent with the data reported by Wei et al. [37] and others [38] who got three weight loss stages at 100 °C by vaporization of water, at 200 °C by elimination of HCl which was used as dopant and at 400 °C by thermal degradation of Polyaniline.

#### 3.3.2. Thermal behavior of pre-heated PAni nano-particles and PAni/$MgFe_2O_4$ core–shell nanocomposite

As shown in Fig. 4a, heating up to 215 °C is favorable for the crystallization of PAni at which its structure becomes more regular and ordered [38], while heating at higher temperatures destroys the crystalline structure. On the other hand pre-heating of PAni prevented the re-crystallization and crosslinking reactions of the polymer chains from appearing in the TGA thermograms, and reduced the amount of HCl loss in the second weight loss step as obvious in the thermal behavior of the pre-heated PAni nano-particles given in Fig. 4b. This is due to the fact that pre-heating caused early re-crystallization and crosslinking and prevents these phenomena from appearing in TGA of pr-heated samples.

Fig. 4c shows that the thermal behavior of the PAni/$MgFe_2O_4$ core–shell nanocomposite differs significantly from that of pure PAni (Fig. 4a), and confirms that some structural change occurs after $MgFe_2O_4$ is incorporated within the PAni matrix. The core–shell nanocomposite undergoes only two weight loss steps with the absence of the second step attributed to re-crystallization due to shortened polymer chains and weaker intra-chain interactions as a result to the presence of $MgFe_2O_4$ in the PAni matrix. The weight losses around 100 °C due to the release of moisture absorption showed systematic decrease both with pre-heating and with introducing the core material into the PAni shell. This is because of the pre-evolution of moisture in the case of pre-heating, and because of the smaller content of polymer obstructed with the $MgFe_2O_4$ in the case of core–shell. The main degradation peak showed similar temperature at the minimum of DrTGA curves for all the PAni's, but the only difference is that the intercalated nanocomposite system showed reduced width and depth for the polymer degradation mechanism, and peaks were getting stronger and sharper. This might be correlated by the macromolecule chains of PAni which become obstructed by magnetic ferrite in the core–shell. This shortens the polymer chains and affects the intra-chain interactions which become weaker due to the presence of $MgFe_2O_4$ in the PAni matrix. As a result, the amorphousity of the polymer increases and degradation of the chains takes place within a lower temperature range than that of pure PAni, which is in consistent with XRD results.

Indeed, TGA results indicate that the thermal stability of the core–shell nanocomposite is better than that of pure PAni and that pre-heated samples showed better thermal stability than the untreated ones. These results indicated that there are some possible types of interaction between the $MgFe_2O_4$ nano-particles and the PAni backbone. $MgFe_2O_4$ nano-particles are believed to effectively act as barriers, which restrict the thermal motion of the PAni chains, and block its re-crystallization and/or crosslinking, and shield the degradation of PAni in the composite. Moreover,

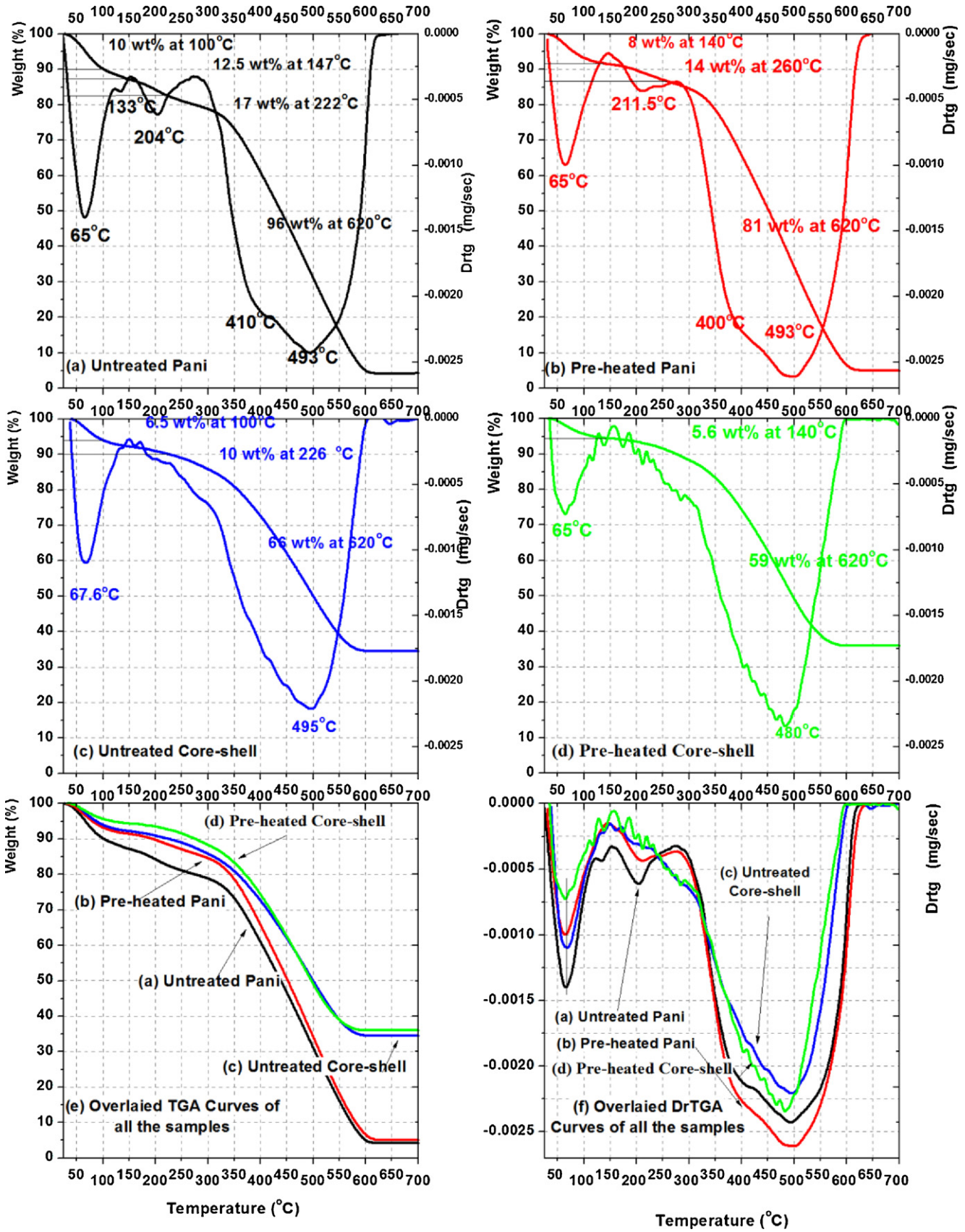


**Fig. 4.** TGA and DrTGA for: (a) un-treated PAni, (b) pre-heated PAni, (c) un-treated PAni/$MgFe_2O_4$ core–shell, (d) pre-heated PAni/$MgFe_2O_4$ core–shell, (e) overlaid TGA curves and (f) overlaid DrTGA curves for all samples.

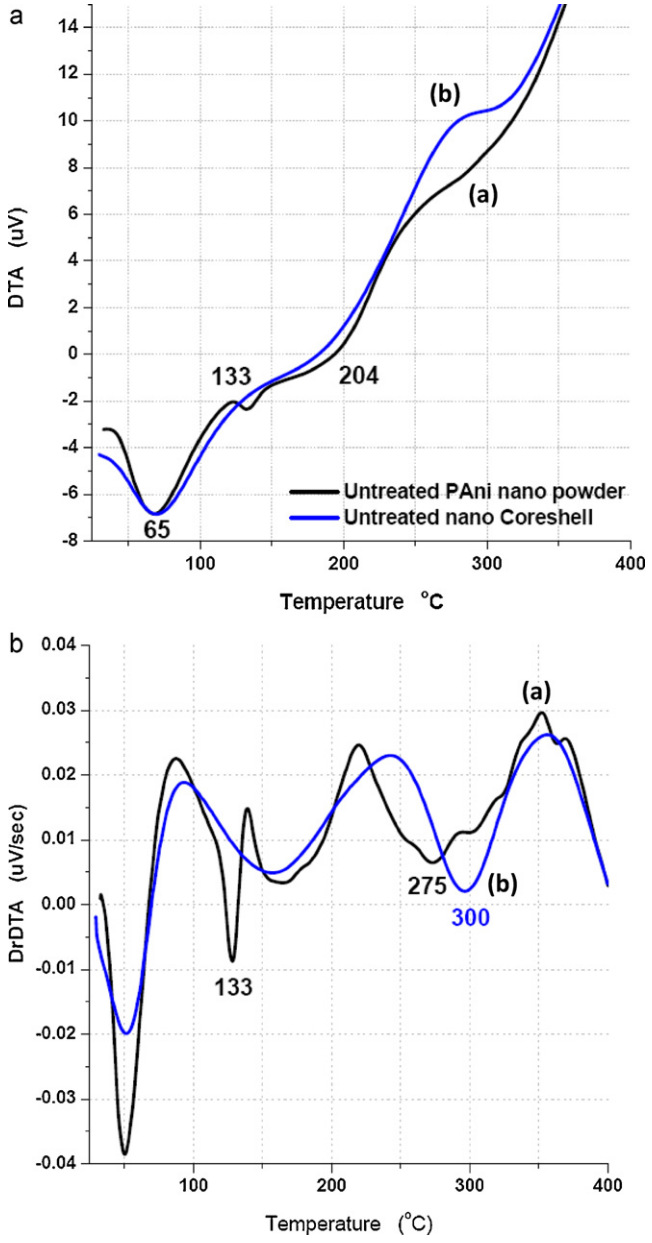


**Fig. 5. (a)** DTA thermograms for: (a) un-treated PAni and (b) un-treated PAni/$MgFe_2O_4$ core–shell. **(b)** DrDTA thermograms for: (a) un-treated PAni and (b) un-treated PAni/$MgFe_2O_4$ core–shell.

it can be learned form Fig. 4e that magnetic ferrite residual material content is approximately 35 wt%, which indicates consistency between the composition of the composite and feed materials.

### 3.3.3. DTA of untreated PAni, and PAni/$MgFe_2O_4$ core–shell nanocomposite

Fig. 5a and b shows the DTA and DrDTA of untreated PAni, and PAni/$MgFe_2O_4$ core–shell nanocomposite respectively. It is well known that the melt processing is not possible for PAni's, since the polymer decomposes at temperatures below its softening or melting point [39]. As compared with PAni, the DTA and DrDTA peaks for PAni/$MgFe_2O_4$ core–shell nanocomposite curve appeared at higher temperature, which is attributed to the interaction between ferrite particles and PAni chains. More over DTA data agrees well with those obtained from TGA measurements.

## 3.4. Changes in the Raman spectra due to thermal degradation

Raman microscope spectroscopy was applied to confirm the TGA and DTA thermal studies as an additional tool for getting more information about the samples under investigation. Pre-heated PAni, and PAni/$MgFe_2O_4$ core–shell nanocomposite samples were investigated by Raman microscopy at two spots each (A and B) and compared to the Raman spectra of the untreated samples built at two spots too as shown in Figs. 6 and 7a, respectively.

### 3.4.1. Raman spectra of pre-heated and untreated PAni

Fig. 6 shows that at spot A of pre-heated PAni, the bands at 1469, 1407, 1152 and 746 $cm^{-1}$ all related to the Quinone vibration were enhanced due to the heating effect. These bands are most probably assigned to the formation of phenazine-like structures, related to the vibrational modes of structures containing nitrogens, which were formed by crosslinking in pre-heated PAni.

On spot B, Raman bands at 1600, 1648, 1240, 541, 490 were enhanced due to pre-heating the sample, and the appearance of new band at 410 $cm^{-1}$ was observed. All of these bands are related to the semi-quinone benzene rings vibration which might be present at spot B.

The origin of the band at 1648 $cm^{-1}$ is corresponding to the occurrence of crosslinked structures induced in the materials due to thermal treatment [40]. The changes in the relative intensity and position of the band 1519 $cm^{-1}$ with respect to the band 1469 $cm^{-1}$ reflects the conformational changes induced by temperature, which might convert PAni from one form to another (most probably the base form).

The increased intensity of the band at 1240 $cm^{-1}$can be associated with the increase in the number of quinonoid and semi-quinonoid rings in the structure due to heating. This is confirmed by the marked increase of the bands at 1500 and 1157 $cm^{-1}$ too, as they correspond to the deformation vibration of the C–H groups on the quinonoid rings. This means that the number of quinonoid and semi-quinonoid rings might increase at a certain spots of the sample due to heating. These results lead to an assumption about the presence of different conjugation chain lengths and types, such as the appearance of the semi-quinones aside the quinone rings in the polymer chain, which showed different response upon heating the sample.

### 3.4.2. Raman spectra of pre-heated and untreated PAni/$MgFe_2O_4$ core–shell nanocomposite

Fig. 7b shows the Raman spectra of pre-heated PAni/$MgFe_2O_4$ core–shell nanocomposite at two spots as compared with the untreated samples. Raman microscopy revealed that pure PAni is less stable than the corresponding core–shell nanocomposite with respect to molecular changes which might occur during heating at elevated temperature. This result agrees well with the TGA and DTA investigations which confirmed that introducing the spinel Ferrite to the core of the polymer enhanced the thermal stability of the nanocomposite. The correlation between stability of the molecular structure and conductivity may certainly be coincidental, yet a possible explanation can be offered.

## 3.5. Magnetic properties

Fig. 8 shows the magnetization, M, versus the applied magnetic field, H, for Polyaniline, $MgFe_2O_4$ and PAni/$MgFe_2O_4$ nanocomposite at room temperature. The magnetization of PAni/$MgFe_2O_4$ nanocomposite exhibits a clear hysteresis behavior. Table 1 gives the magnetic parameters including saturation magnetization (Ms), coercivity (Hc) and remnant magnetization (Mr) determined from the hysteresis loops measurements. The values Ms, Mr and Hc for PAni/$MgFe_2O_4$ composite are less than those obtained for pure

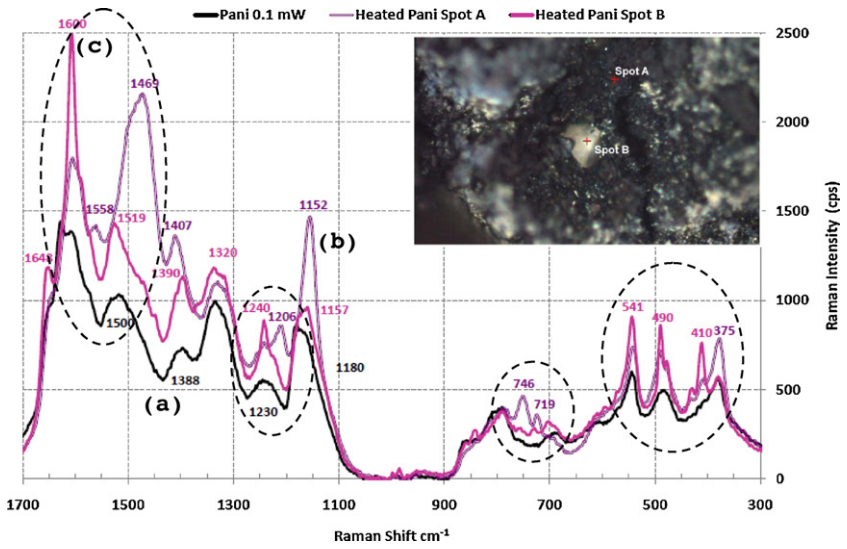


**Fig. 6.** Raman microscope spectra for: (a) un-treated PAni, (b) pre-heated PAni built at spot A and (c) pre-heated PAni built at spot B.

$MgFe_2O_4$. According to the equation Ms = $\varphi$mS, where $\varphi$ is the volume fraction of the particles and mS is the saturation moment of a single particle, it is clear that Ms of the nanocomposite is dependent on the volume fraction of the magnetic ferrite particles ($\varphi$), and on the contribution of the non-magnetic PAni coating layer to the total magnetization. PAni/$MgFe_2O_4$ nanocomposite has less magnetization than that observed for the pure magnesium ferrite nano-particles, which means that the total magnetic behavior of the nanocomposite could be tuned and tailored depending on these two parameters.

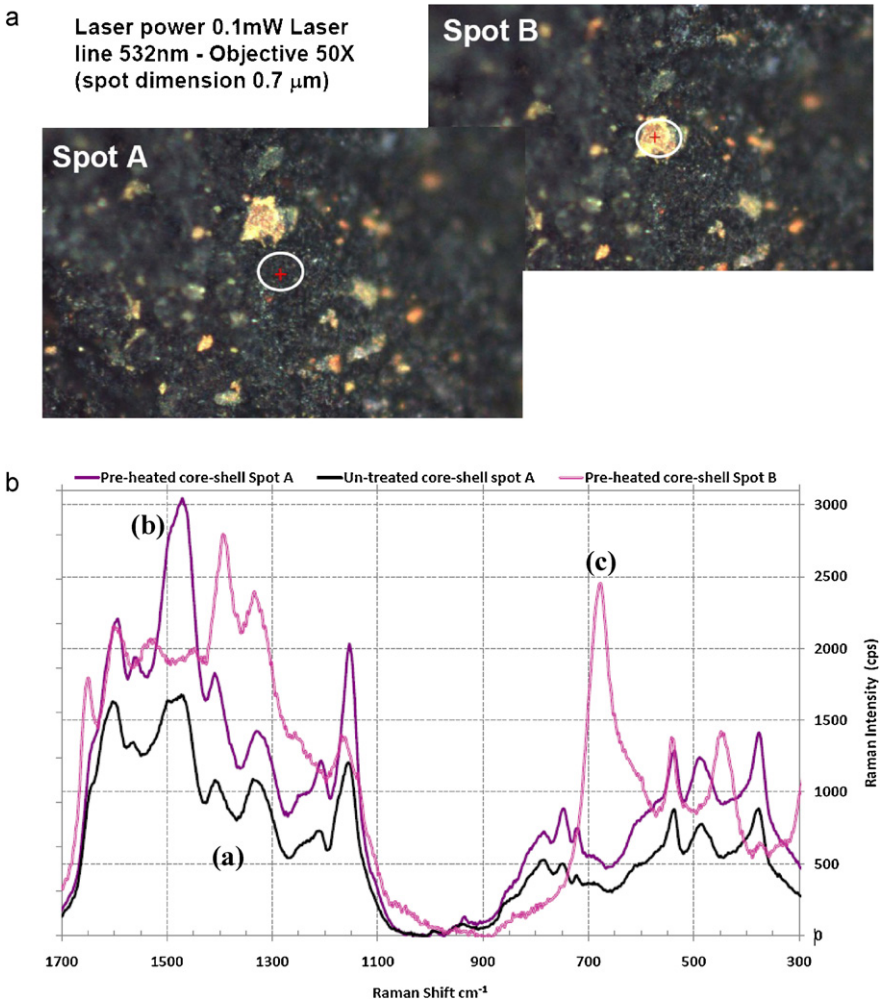


**Fig. 7. (a)** Raman microscope image built at spot A and spot B for pre-heated PAni/$MgFe_2O_4$ core–shell. **(b)** Raman microscope spectra for: (a) un-treated PAni/$MgFe_2O_4$ core–shell, (b) pre-heated PAni/$MgFe_2O_4$ core–shell built at spot A, (c) pre-heated PAni/$MgFe_2O_4$ core–shell built at spot B.

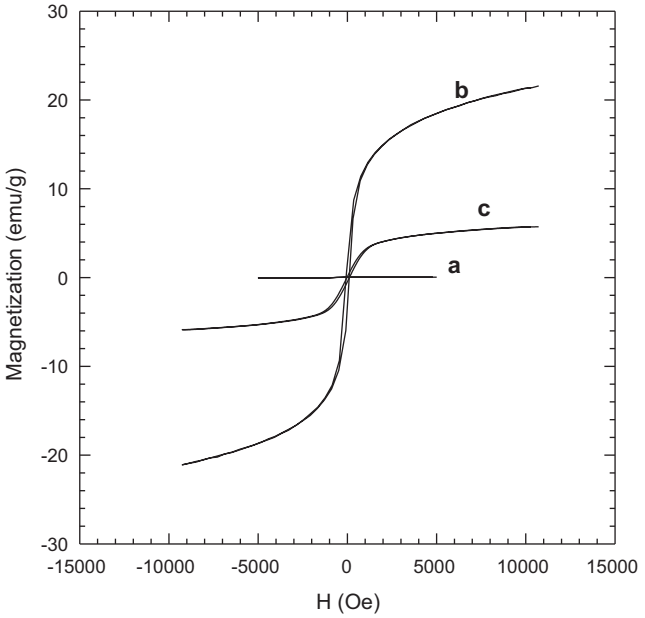


**Fig. 8.** Magnetization hysteresis loops for: (a) PAni, (b) $MgFe_2O_4$, and (c) PAni/$MgFe_2O_4$ core–shell.

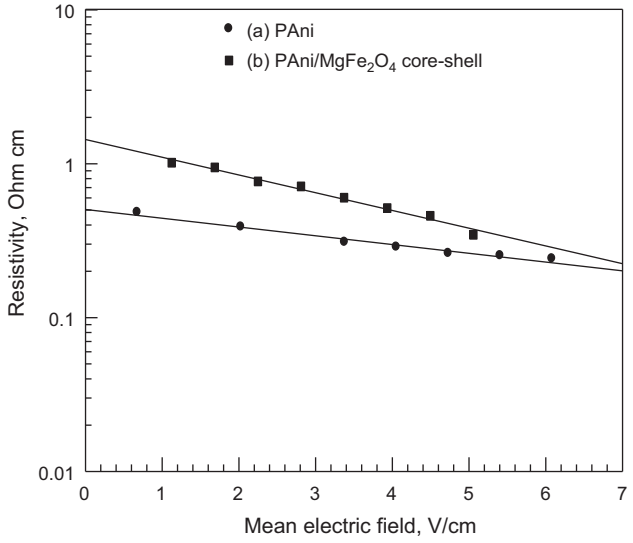


**Fig. 9.** Resistivity of: (a) PAni and (b) PAni/$MgFe_2O_4$ core–shell versus the mean electric field.

Moreover, the coercivity is dependent on the microstructure of PAni/$MgFe_2O_4$ nanocomposite. It is well known that polycrystalline ferrites have an irregular structure, geometric and crystallographic nature, such as pores, cracks, surface roughness and impurities. In the polymerization process, depositing PAni on the ferrite surface and crystallite boundary, has a healing effect to cover the ferrite surface defects, such as pores and cracks, leading to a decrease in magnetic surface anisotropy of ferrite particles, consequently, PAni/$MgFe_2O_4$ nanocomposite presents a lower value of coercivity than that of $MgFe_2O_4$.

### 3.6. The resistivity and its electrical field coefficients of pure PAni and PAni/$MgFe_2O_4$ nanocomposite

Intrinsically conducting polymers (ICPs), among them PAni are inherently conducting in nature due to the presence of a conjugated π electron system in their structure. Also, PAni is not charge conjugation symmetric, which means that the valence and conduction bands are asymmetric to a great extent [18]. The partial oxidation of PAni usually leads to the reorganization of bonds, resulting in an increase in electronic conductivity. Hence, conductivity of PAni can be influenced and tuned both by changing the charging level and the degree of protonation.

The log resistivity of PAni and PAni/$MgFe_2O_4$ nanocomposite was plotted against mean DC electrical field for the two samples at 25 °C (Fig. 9). It is clear from Fig. 9 that the resistivity is electrical field dependent. For all samples, the log resistivity decreases approximately linearly with applied electrical field. The electrical field dependence of resistivity can be described by the following equation:

$$\rho = \rho_0 \exp(-\beta E)$$

**Table 1**
Magnetic parameters of PAni, $MgFe_2O_4$ and $MgFe_2O_4$/PAni core shell nanocomposite.

| Sample | Ms (emu/g) | Mr (emu/g) | Hc (Oe) |
|---|---|---|---|
| PAni | 0.0463 | 0.01051 | 18.97 |
| $MgFe_2O_4$ | 21.33 | 2.108 | 88.66 |
| PAni/$MgFe_2O_4$ core shell | 5.905 | 0.6659 | 81.6 |

where $E$ is the electrical field, $\beta$ is the electrical field coefficient of resistivity and $\rho_0$ is a constant corresponding to resistivity at very small electrical field. By fitting a straight line to the log resistivity versus electrical field data, the electrical field coefficient of resistivity ($\beta$) could be obtained from the gradient. Calculations showed that $\beta = 0.057$ cm/V for PAni and $\beta = 0.115$ cm/V for PAni/$MgFe_2O_4$ core–shell nanocomposite. It can be seen that PAni has a relatively smaller electrical field coefficient than the core–shell nanocomposite. Fig. 9 also shows that at early electric field stages the resistivity of PAni is smaller than that of the core–shell nanocomposite, but at late stages, and upon extrapolating the straight lines, one will notice that the resistivity of the core–shell nanocomposite approached that of PAni and exceed it in an opposite direction. This means that at a threshold mean electric field, the core–shell PAni/$MgFe_2O_4$ nanocomposite will show smaller resistivity and higher conductivity than that for PAni itself. In other words, adding the magnetic ferrite core to the PAni shell leads to enhancing the conductivity of the core–shell sample after certain threshold voltage.

## 4. Conclusion

Conductive and magnetic Polyaniline/$MgFe_2O_4$ nanocomposite was successfully synthesized in the form of core–shell via in situ chemical polymerization of aniline in the presence of $MgFe_2O_4$ nano-particles. XRD, Raman and thermal studies suggests that PAni undergoes interfacial interactions with $MgFe_2O_4$ crystallites and loses its own morphology by coating the magnetic ferrite nanoparticles, implying that there is no strong chemical interaction between PAni and $MgFe_2O_4$ in the prepared core–shell nanocomposite. The thermal stability of the core–shell nanocomposite is better than that of pure PAni and pre-heated samples showed better thermal stability than the untreated ones. PAni/$MgFe_2O_4$ core–shell nanocomposite has less magnetization, coercivity and resistivity together with better conductivity after certain threshold applied voltage than that observed for the pure magnesium ferrite nano-particles. This means that the total magneto-electrical behavior of the nanocomposite could be tuned and tailored depending on the volume fraction of the magnetic ferrite particles ($\varphi$), and on the contribution of the non-magnetic PAni coating layer.

## Acknowledgements

The author is very much thankful to the Materials Science Laboratory Group, Chemistry Department, Faculty of Science, Beni-Suef University, Egypt, for their assistance in preparing the materials used in the present study.

The author also acknowledges ThermoFisher Scientific, Italy, for performing Raman microscope measurements found in this publication.

## References

[1] M.L. Singla, S. Awasthi, A. Srivastava, D.V.S. Jain, Sens. Actuators A 136 (2007) 604–612.
[2] A.A. Farghali, M. Moussa, M.H. Khedr, J. Alloys Compd. 499 (2010) 98–103.
[3] G. Li, S. Yan, E. Zhouc, Y. Chena, Colloids Surf. A: Physicochem. Eng. Aspects 276 (2006) 40–44.
[4] H. Kawaguchi, Prog. Polym. Sci. 25 (2000) 1171.
[5] O. Kalinina, F. Kumacheva, Macromolecules 32 (1999) 4122.
[6] G.R. Pedro, Adv. Mater. 13 (3) (2001) 163.
[7] R.H. Marchessault, P. Rioux, L. Raymond, Polymer 33 (1992) 4024.
[8] R.F. Ziolo, E.P. Fiannelis, B.A. Weistein, et al., Science 257 (1992) 219.
[9] A. Dhanabalan, S.S. Talwar, A.Q. Contractor, et al., J. Mater. Sci. Lett. 18 (1999) 603.
[10] B. Wessling, ACS Symp. Ser. 843 (2003) 34–73.
[11] Z. Guo, K. Shin, A.B. Karki, D.P. Young, R.B. Kaner, H.T. Hahn, J. Nanoparticle Res. 11 (6) (2009) 1441–1452.
[12] J. Zhu, S. Wei, A. Max Jr., T.D. Dang, T.C. Ho, Z. Guo, J. Phys. Chem. C 114 (39) (2010) 16335–16342.
[13] J. Zhu, S. Wei, L. Zhang, Y. Mao, J. Ryu, A.B. Karki, D.P. Young, Z. Guo, J. Mater. Chem. 21 (2011) 342–348.
[14] M.X. Wan, J.H. Fan, J. Polym. Sci. Part A: Polym. Chem. 36 (1998) 2749.
[15] M.X. Wan, W.C. Li, J. Polym. Sci. Part A: Polym. Chem. 34 (1997) 2129.
[16] J. Stejskal, M. Trchová, J. Brodinová, P. Kalenda, S.V. Fedorova, J. Prokeš, J. Zemek, J. Colloid Interface Sci. 298 (2006) 87–93.
[17] A. Mirmohseni, A. Oladegaragoze, M. Farbodi, Iran. Polym. J. 17 (2) (2008) 135–140.
[18] S. Bhadra, D. Khastgir, N.K. Singha, J.H. Lee, Prog. Polym. Sci. (2008), doi:10.1016/j.progpolymsci.2009.04.003.
[19] Z.L Wang, Y. Liu, Z. Zhang, Handbook of Nanophase and Nanostructured Materials, vol. 3, Kluwer Academic/Plenum Publishers, New York, 2002.
[20] F. Wang, S.X. Min, Chin. Chem. Lett. 18 (2007) 1273.
[21] H. Zhang, Q. Qi, D.G. Evans, X. Duan, J. Solid State Chem. 177 (2004) 772.
[22] X. Duan, Q.Z. Jiao, Chinese Patent CN 00132145.5, 2000.
[23] Y. Zhao, F. Li, R. Zhang, D.G. Evans, X. Duan, Chem. Mater. 14 (2002) 4286.
[24] J. Jiang, L. Li, F. Xu, Mater. Sci. Eng. A 456 (2007) 300.
[25] J.P. Pouget, M.E. Jozefowicz, A.J. Epstein, X. Tang, A.G. Macdiarmid, Macromolecules 24 (1991) 779.
[26] Q. Li, L. Cruz, P. Philips, Phys. Rev. B 47 (1993) 1840–1845.
[27] W.B. Cross, L. Affleck, M.V. Kuznetsov, I.P. Parkin, Q.A. Pankhurst, J. Mater. Chem. 9 (1999) 2545.
[28] F.A. Radwan, M.A. Ahmed, G. Abdelatif, J. Phys. Chem. Solids 64 (2003) 2465.
[29] M.A. Ahmed, G. Abd-Ellatif, M. Rashad, J. Magn. Magn. Mater. 232 (2001) 194.
[30] J.P. Pouget, M.E. Józefowicz, A.J. Epstein, X. Tang, A.G. MacDiarmid, Macromolecules 24 (1991) 77–89.
[31] H.K. Chaudhari, D.S. Kelkar, J. Appl. Polym. Sci. 63 (1996) 8–15.
[32] F. Fusalba, D. Bélanger, J. Mater. Res. 14 (1999) 1805–1813.
[33] Q.H. Zeng, D.Z. Wang, A.B. Yu, G.Q. Yu, Nanotechnology 13 (2002) 549–553.
[34] J.P. Pouget, C.H. Hsu, A.G. MacDiarmid, A.J. Epstein, Synth. Met. 69 (1995) 119–120.
[35] H.P. Klug, L.E. Alexander, X-ray Diffraction Procedures for Polycrystalline and Amorphous Materials, Wiley, New York, 1954.
[36] D. Kumar, R. Chandra, Indian J. Eng. Mater. Sci. 8 (4) (2001) 209–214.
[37] Y. Wei, G.W. Jang, K.F. Hsueh, E.M. Scherr, A.G. MacDiarmid, A.J. Epstein, Polymer 33 (2) (1992) 314–322.
[38] T.C. Tsai, D.A. Tree, M.S. High, Ind. Eng. Chem. Res. 33 (1994) 2600–2606.
[39] R. Ansari, M.B. Keivani, E-J. Chem. 3 (2006) 202–217.
[40] M.C. Bernard, A. Hugot-Le Goff, S. Joiret, N.N. Dinh, N.N. Toan, J. Electrochem. Soc. 146 (1999) 995.